Materials Science and Engineering A 397 (2005) 84–91

MATERIALS SCIENCE & ENGINEERING A

www.elsevier.com/locate/msea

Crack initiation and propagation close to the interface in a ferrite–austenite joint

J. Besson[a,*], Y. Madi[a], A. Motarjemi[b,c], M. Koçak[b], G. Martin[d], P. Hornet[d]

[a] *Ecole des Mines de Paris, Centre des Matériaux, UMR CNRS 7633, BP 87, 91003 Evry Cedex, France*
[b] *Institute of Materials Research, GKSS Research Center, Geesthacht 21502, Germany*
[c] *Structural Integrity Group, TWI, Granta Park, Great Abington, Cambridge CB1 6AL, UK*
[d] *EdF les Renardieres, Route de Sens - Ecuelles, 77250 Moret-sur-Loing, France*

Received 28 June 2004; received in revised form 21 January 2005; accepted 26 January 2005

Abstract

The safety assessment of welded structures and joints still remains an important industrial problem. In this study, a simple diffusion bonded bi-material joint has been made in order to analyze the plastic mismatch effect. It consists of an assembly of ferritic and austenitic steels which are representative of nuclear pressure vessel components. Tests were performed on various specimens including smooth and notched tensile bars, Charpy V-notch specimens and single-edge notch bend specimens. Homogeneous and bimaterial specimens were tested. On deeply notched specimens, the effect of the distance between the notch root and the interface on fracture initiation and crack propagation direction was studied. Tests were modeled using elasto-plastic finite element simulations. These simulations were post-processed in order to determine crack initiation based on the Rice and Tracey criterion according to the "local approach of fracture" procedure.

Keywords: Mismatch effect; Welded joints; Ductile fracture; Rice and Tracey model; Finite element simulation

1. Introduction

The structural safety assessment of welded structures (particularly bi-material components) remains an important industrial problem. The interaction between the welded parts, the weld metal and the heat affected zones makes the structural integrity analysis difficult. Geometrical details of the weld may make the problem even more complex.

Two common approaches to fracture that are usually used to analyze rupture of homogeneous elastic–plastic solids are the "global approach" (which started in the 70's) and the "local approach" (which started in the 80's). Applications to heterogeneous structures are more recent. The global approach examines the changes in the crack driving force in terms of the *J*-integral [1], which may be related to the energy release rate. Recently, the effect of the *Q*-factor [2,3], which accounts for scaling the stress triaxiality depending on the crack tip constraint, has been emphasized. The two parameters *J*–*Q* can be used to analyze the stress–strain field close to an interface between plastically dissimilar materials [4,5]. A three parameters approach (so called *J*–*Q*–*M*) has been recently proposed to analyze strength mismatched joints [6]. The need for a three parameters approach outlines the complexity of the situation to be analyzed. The second approach, referred to as local approach, has been developed in particular by the Beremin group [7,8] and considers the local stress and deformation contributions to the failure processes. This approach is able to deal with situations where no preexisting crack is present and to predict the location of crack initiation. In addition, it can be applied without any modification to welds and interfaces thus appearing as an attractive alternative to the global approach in these situations. An example of application to the brittle fracture of welds is given in [9]. Both approaches have been compared for homogeneous materials in [10,11] and for heterogeneous structures in [5] showing that consistent results are obtained in case of cracked structures.

* Corresponding author. Tel.: +33 01 60763000; fax: +33 01 60763150.
E-mail address: jacques.besson@ensmp.fr (J. Besson).

0921-5093/$ – see front matter © 2005 Elsevier B.V. All rights reserved.
doi:10.1016/j.msea.2005.01.056

In this study, a simple diffusion bonded bimaterial joint was produced in order to analyze the strength mismatch effect on damage process at the interface region. It consists of an assembly of ferritic and austenitic steels which are representative of bi-material components used in nuclear pressure vessels. In that case, the joint is welded so that the situation to be analysed is more complex. The bonded joint studied in this work is therefore a simplified representation of the actual structure. The microstructures of each material are first presented. The interface region was analyzed using microprobe analysis. Then the mechanical and fracture behaviors are studied using smooth and notched tensile bars (NT), Charpy V-notch specimens and single edge eotch bend (SENB) specimens. Crack paths and failure mode under static loading are then examined. Results are finally interpreted and modeled using a simple local approach type model for ductile failure.

2. Materials

The study was performed on a bi-material joint consisting of a ferritic (A508) and an austenitic (316L) steels. The bond was processed under the following conditions: 980 °C under a pressure of 8 MPa during 35 min. This processing route leads to specific microstructures and mechanical properties which significantly differ from those of the original materials. In particular the ferrite becomes harder and more brittle due to the thermal cycle of the joining process. Similar results have been found in [12,13] where it was shown that the transition region was shifted from the range −100 to 0 °C to the range 10 to 80 °C after heat treatment.

The ferritic–austenitic joints in the current study were not post-bond heat treated to restore the initial properties in order to keep the interdiffusion zone as small as possible. A batch of ferrite material was also submitted to the same heat treatment as the joints have experienced during the bonding process. This bulk material can be characterized to obtain reference properties of the ferrite.

The nominal chemical compositions of both steels are listed in Table 1. Microprobe analysis (Cameca SX50) were carried out across the interface to characterize the interdiffusion profiles. A micrograph of the interface is shown in Fig. 1. The diffusion bonding process leads to element migration across the interface. Austenitic grains are marked by carbides over a distance of about 100 μm. This is well corroborated by carbon profiles across the interface which indicate a carbon diffusion depth of about 40 μm. For elements other than carbon (Si, Cu, Mo, Mn, Cr and Ni), microprobe profiles across the interface indicate a sharper transition which extends over less than 10 μm. The microprobe analysis maps of the interface show some particles identified as oxides containing manganese, silicon and chromium. These particles may embrittle the interface (Table 2).

Table 1
Nominal chemical compositions of the materials (wt.%)

	C	S	P	Si	Mn	Ni	Cr	Mo	Cu
A508	0.19	0.01	0.01	0.19	1.52	0.55	0.18	0.49	0.07
316L	0.03	0.04	0.03	0.51	1.88	12.0	18.0	2.52	0.38

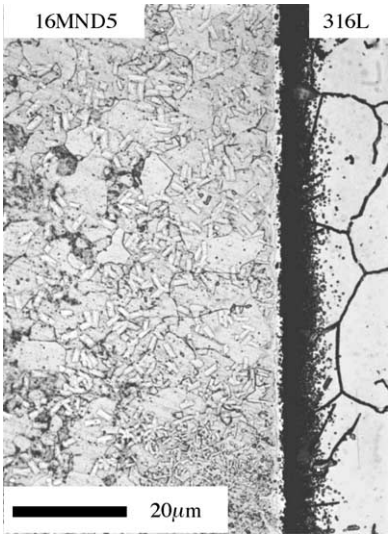

Fig. 1. Optical micrograph showing the interface and austenitic grain boundaries decorated with carbides.

3. Test samples and testing conditions

Mechanical tests were carried out on homogeneous ferritic materials (which have been subjected to the same heat treatment as the joints) and bimaterial joints. Monolithic austenite samples were not available for bulk material property characterization. However, sub-sized specimens were used to obtain some properties. Several specimen types were used to characterize the materials. This includes: (i) smooth tensile bars, (ii) U-notched tensile bars (Fig. 2), (iii) V-notched tensile bars (Fig. 2), (iv) sub-size Charpy specimens (Fig. 3(a)) and single edge notch bend specimens (Fig. 3(b)). These specimens are respectively referred to as: TB, NT_χ, ($\chi = 10 \times r/\phi_0$, where r is the notch radius and ϕ_0 the sample diameter at the minimum cross section), NT_V, KCV and SENB. For tests performed on homogeneous specimen, the specimen name is followed by a letter "F" for ferrite or by a letter "A" for austenite in order to identify the material. Standard tensile properties for both materials are given in Table 2.

In the case of heterogeneous specimens, the notch plane is always parallel to the interface. In this case, the letter

Table 2
Tensile mechanical properties of both materials

	$R_{p0.2}$ (MPa)	R_m (MPa)	A (%)
A508	568	770	8
316L	264	601	43
Mismatch (A508/316L)	2.15	1.28	0.18

Data for the austenite were deduced from the analysis of sub-sized notched tensile specimens.

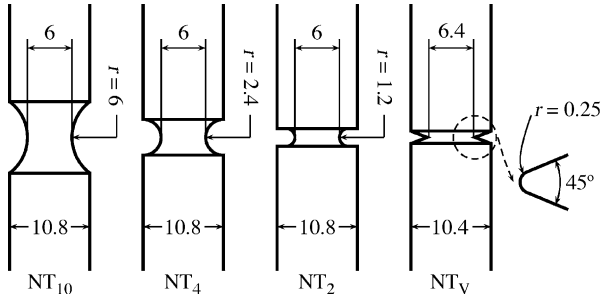

Fig. 2. Axisymmetric notched specimens (NT_χ and NT_V).

identifies the material in which the notch lies and a number gives the distance between the notch and the interface. The letter "I" is used to show that the interface between both materials lies at the notch tip. For instance the designation KCV1F represents a Charpy specimen whose notch tip is in the ferrite at a distance of 1 mm from the interface.

All tests were carried out at room temperature. TB samples were tested with a strain rate equal to $10^{-3}\,s^{-1}$. NT_χ samples were tested with controlled radial displacement of the minimum cross section in order to get an average strain rate in the notch equal to $10^{-3}\,s^{-1}$. In the case of heterogeneous NT_χ specimens axial displacement was measured with an extensometer (gage length of 10 mm) which was located symmetrically on both sides of the notch (Fig. 4(b)). Some sub-size samples NT (minimum diameter: 4 mm) were extracted from the diffusion bonded block (see Fig. 4(a)). They remain much larger than the material grain size. This served two purposes: (i) verifying that the behavior of

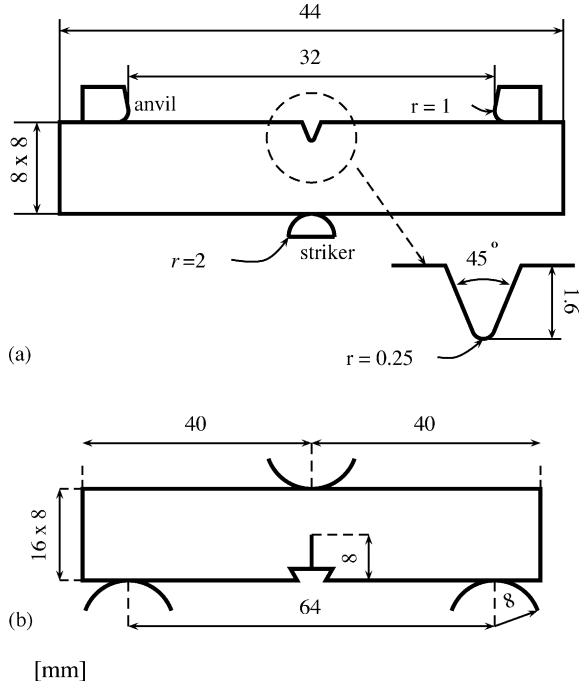

Fig. 3. (a) Sub-size Charpy specimens. (b) SENB specimen (thickness $B = 8$ mm).

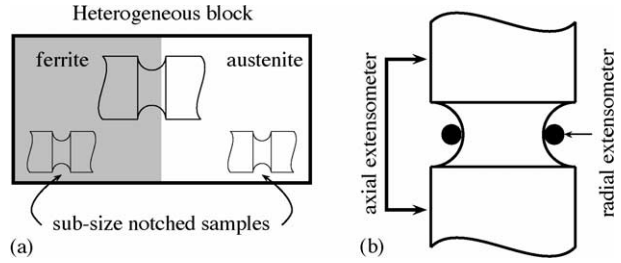

Fig. 4. (a) Notched samples extracted from diffusion bonded heterogeneous blocks. (b) Axial and radial extensometers on NT_χ and NT_V samples.

the ferritic material extracted from the bonds is similar to that of the heat treated homogeneous material, (ii) obtaining some information about the plastic and rupture behavior of the bulk austenite. The notch opening was measured with a 10 mm gage length. NT_V samples were tested with a constant load line velocity of $6.5\,\mu m s^{-1}$. The axial displacement was measured in a similar way as for the NT_χ specimens using a gage length of 13 mm. Due to limited amount of material available, Charpy specimens used in this study are slightly smaller than the standard ones [14]. The sample geometry as well as the geometry of the anvil and the striker are detailed in Fig. 3(a). The tests were carried out under quasi-static conditions using a load line velocity of $20\,\mu m s^{-1}$. In both previous cases, the load line velocity was selected in such a way to obtain strain rates close to $10^{-3}\,s^{-1}$ in the notch region. SENB specimens contain sharp cracks which were produced by fatigue with a stress intensity factor amplitude of 20 MPa $\sqrt{m}$. They were then tested with a load line velocity of 1 mm/mn. The crack mouth opening displacement (CMOD) was measured during the test.

4. Crack paths and fractographic examinations

Fractographic examinations of different samples were conducted in order to investigate: (i) the failure mechanisms, (ii) the crack path and crack deflection.

Fig. 5(a) and (b) show cross sections of samples NT_2I (stopped before failure) and $NT_{10}I$ whose failure occurred in the austenite where damage by void growth took place. Fracture surfaces for the austenite show large dimples (100 μm). Fig. 5(c) shows the ductile crack initiation zone in the ferrite in sample NT_V3F followed by cleavage areas. Dimples in the ductile region are relatively small (5–10 μm).

Due to the strength mismatch, the development of strains and stresses is no longer symmetric in heterogeneous samples. This causes crack deflection from the usually observed path on homogeneous samples. This effect is illustrated on Fig. 6 in the case of KCV samples. It is shown that in cases where the notch lies in the ferrite, the crack is deviated toward the interface for KCV1F and KCV2F specimens where notch tip distance was 1 and 2 mm, respectively. In the case of the KCV4 ··· 9F specimens the crack runs

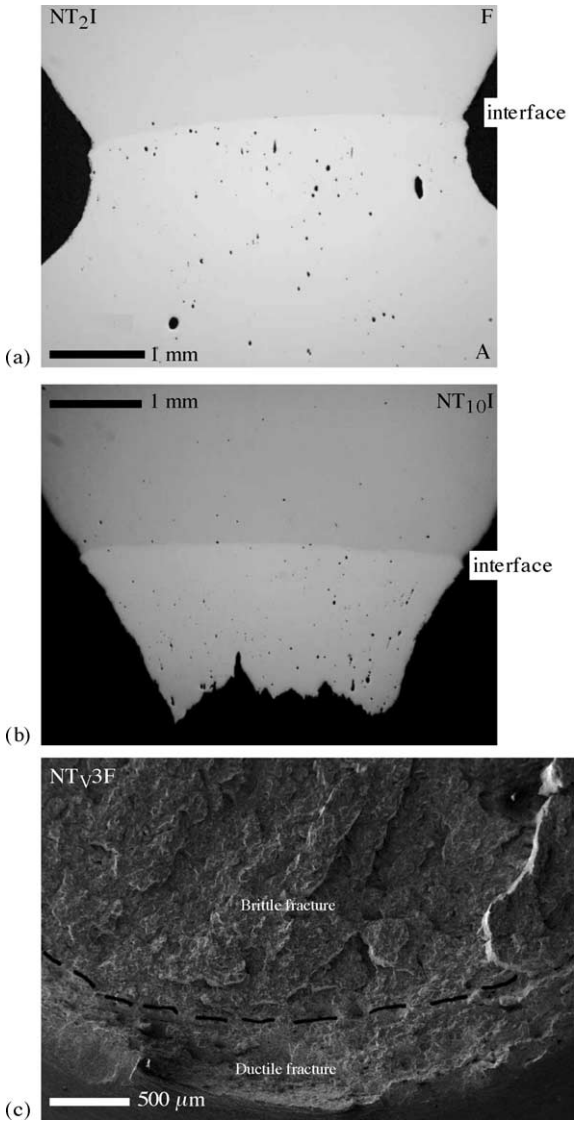

Fig. 5. Fractographic examination: (a) cross section of a NT_2I sample showing ductile damage development in the austenite before failure, (b) cross section of a $NT_{10}I$ sample after failure showing damage and the fracture surface in the austenite. (c) SEM examination of a NT_V3F sample fracture surface showing ductile failure initiation followed by brittle failure. The dashed line indicates the transition between ductile and brittle fracture.

straight, since the interaction of neighboring materials is not any more effective on the fracture process. For the KCV1F specimen, final failure occurred by interface failure. In the case of the KCV2F sample, the interface is crossed by the running crack which further propagates into the austenite. In the case of KCV#A specimens the opposite effect is observed. For KCV1A specimens, the crack tends to propagate away from the interface. The effect is reduced for KCV2A specimens. Otherwise the crack runs straight (KCV4A). Very similar and consistent trends were observed on SENB specimens. Such an example is given in Fig. 7(a) for the case of a SENB2F sample which shows cracks deflection toward the interface.

5. Results of mechanical tests

5.1. Results for smooth and notched bars

Results for homogeneous ferrite on smooth (TB) and notched tensile bars are shown in Fig. 8(a). The load increases and ductility decreases with increasing notch severity as usually reported [15]. Failure in sample NT_2F is initiated at the center of neck region of the specimens. In this particular case, initiation is ductile but outside the central region failure becomes brittle thus explaining the rapid load drop. All other samples have a fully ductile failure mode. $NT_{10}F$ sub-size samples (extracted from bonded blocks) were also tested (dashed lines on Fig. 8(a)). In comparison with full size specimens from homogeneous blocks, the sub-size samples showed similar plastic behavior. Failure initiation (indicated by the rapid load drop) is scattered although the failure mechanism is fully ductile. This observation is consistent with other studies with respect to existing scatter and size effect on ductile failure on a similar material [16]. Therefore, it can be concluded that the ferritic materials in homogeneous blocks and in bonded joints are similar, since both materials have experienced identical thermal cycles and exhibit similar plastic properties.

Fig. 8(b) shows results obtained on a sub-size $NT_{10}A$ austenitic specimen. These data can be used to determine the plastic behavior of the austenitic material using an inverse identification method (Section 6.1) [17].

Results obtained from heterogeneous samples are shown in Fig. 9. Several NT_χ samples were tested. However, most of them resulted in interface failure which is out side of the scope of this work. Fig. 9(a) shows force–displacement curves for samples NT_2I and $NT_{10}I$ in which failure occurred in the austenite. The usual notch effect is observed: load is increased with increasing notch severity whereas ductility is decreased. Results for NT_V samples are shown in Fig. 9(b). Due to the sharp notch, failure is always initiated at the notch root. When the notch is located in the ferrite ($NT_V2F\cdots NT_V6F$), decreasing distance to the interface causes the apparent ductility to increase and the maximum load to decrease. The ductility increase is partially caused by the deformation of the austenite along the 13 mm gage length. In all cases, stable crack growth initiated at the notch root (which can be observed visually) and preceded final failure.

5.2. Results for Charpy specimens

Results for Charpy specimens are shown in Fig. 10 for samples with the notch located in the ferrite and in Fig. 11 for samples with the notch located in the austenite. Specimens KCVF, KCV9F and KCV4F have very similar behaviors showing that the interface is too far from the notch root to influence the response of the bimaterial structure. In these cases, failure initiation corresponds to a ductile mechanism

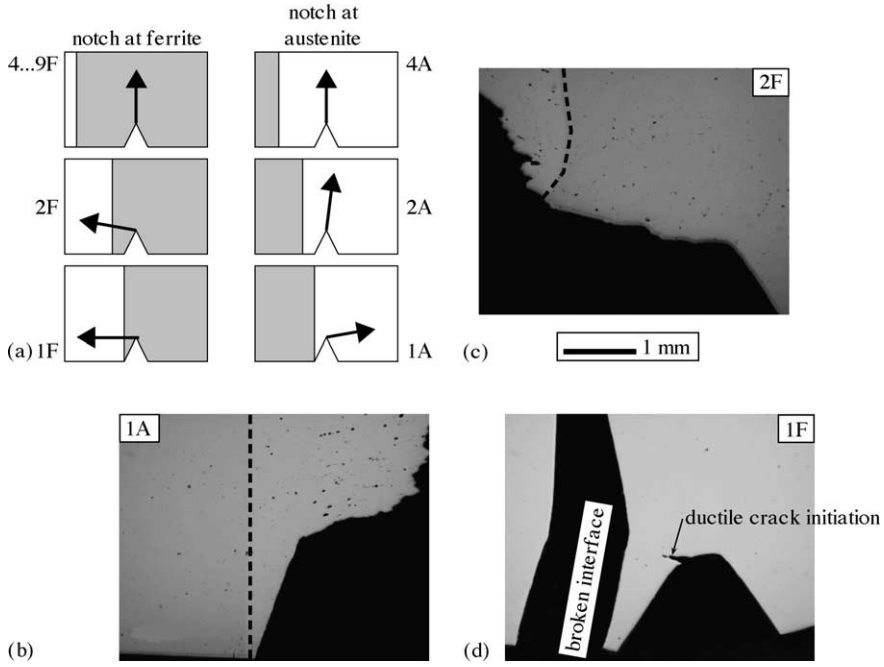

Fig. 6. Crack paths (arrows) observed on Charpy specimens for different locations (A and F) and distances between the notch tip and the interface. Schematic (a) is showing the fracture paths developed with respect to different locations and distances to the bi-material interfaces, (b) notch in austenite at a distance of 1 mm, (c) and (d) notch in ferrite at distances of 2 and 1 mm, respectively. The dashed line delineates the ferrite/austenite interface.

but is followed by brittle failure. Deformation to failure is increased for specimens KCV2F and KCV1F. As in the case of NT_V specimens the maximum load is reduced. The early failure of specimen KCV1F is caused by interface failure (Fig. 6). Specimens KCV4A and KCV2A showed a similar behavior which implies that the presence of the interface plays a limited role on the fracture performance. On the other hand, specimen KCV1A appears to be affected and fails rapidly.

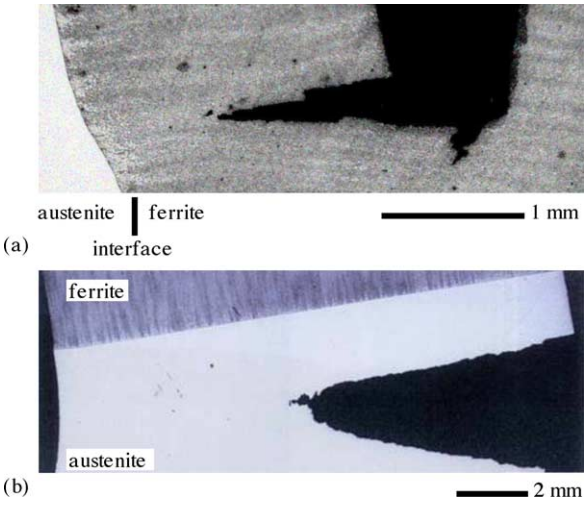

Fig. 7. (a) Crack path observed on an SENB2F specimen showing crack deflection toward the interface (Nital etching), (b) crack path observed on an SENB2A specimen showing that the crack remains flat and that crack advance is limited (CMOD = 2.8 mm, Nital etching).

5.3. Results for SENB specimens

Results obtained from SENB specimens (Fig. 12) indicate the same trends as for the Charpy specimens containing blunt-notches and tested under static loading. The homogeneous SENBF specimen fails rapidly with ductile crack initiation and subsequent brittle fracture. Bi-material specimen SENB2F showed much higher ductility although the maximum load was similar. This indicates the beneficial effect of the austenite in heterogeneous joints when the notch tip is in the ferrite. By stopping the test before final failure, specimen SENB2A showed a very limited crack growth up to 3 mm CMOD. This shows good resistance of the austenite to crack propagation.

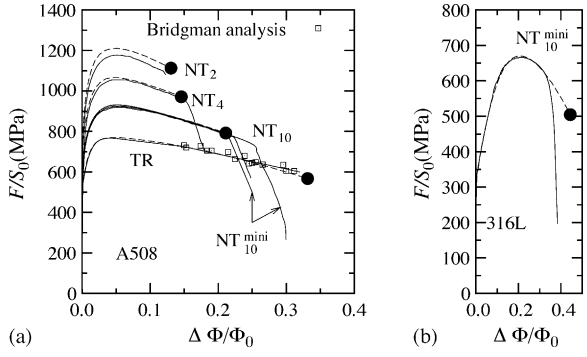

Fig. 8. Testing of axisymmetric notched specimens: (a) results for homogeneous ferrite, (b) results for austenite. (F: force, S_0: initial cross section, ϕ_0: initial minimum diameter, $\Delta\phi$: variation of the minimum diameter). Dashed lines correspond to the FE simulation. Black dots indicate the predicted fracture initiation.

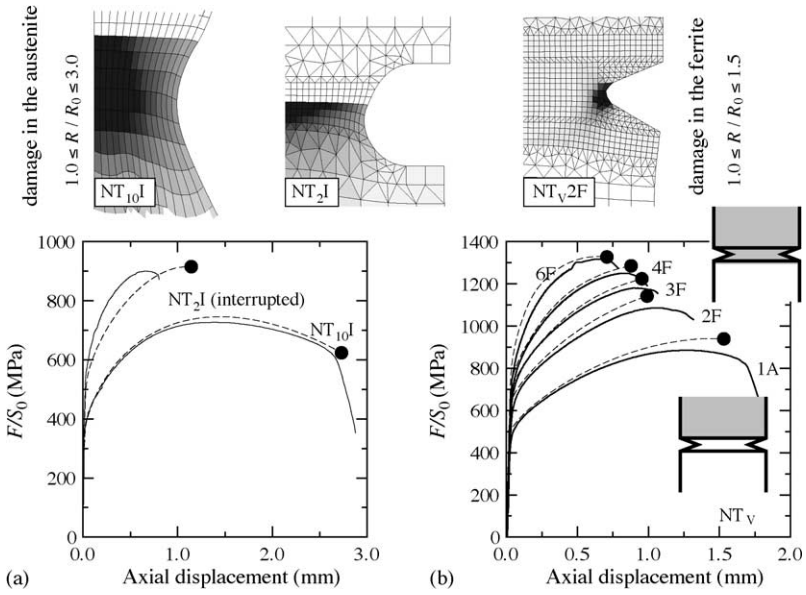

Fig. 9. Testing of axisymmetric bimaterial notched specimens: (a) Results for $NT_{10}I$ and NT_2I specimens, (b) results for NT_V specimens. Dashed lines correspond to the FE simulation. Black dots indicate the predicted fracture initiation. Maps show the damage indicator at predicted crack initiation.

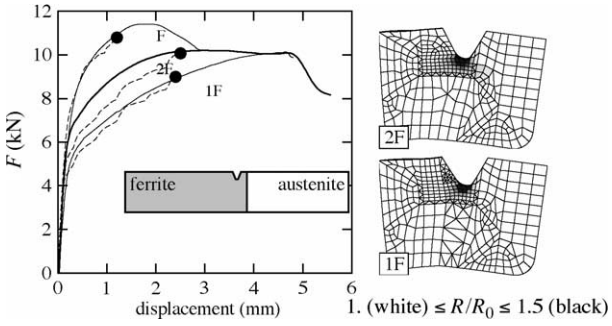

Fig. 10. Charpy tests under static loading: force–deflection curves for samples whose notches are in the ferrite for different values of the distance between the notch tip and the interface. Dashed lines correspond to the FE simulation. Black dots indicate the predicted fracture initiation in the ferrite. Maps show the damage indicator at predicted crack initiation computed in the ferrite.

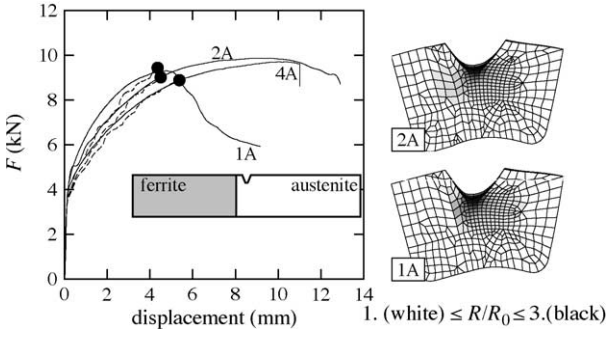

Fig. 11. Charpy tests under static loading: force–deflection curves for samples whose notches are in the austenite for different values of the distance between the notch tip and the interface. Dashed lines correspond to the FE simulation. Black dots indicate the predicted fracture initiation in the austenite. Maps show the damage indicator at predicted crack initiation computed in the austenite.

6. Simulation—discussion

In this section, an interpretation of the main experimental results is proposed based on an application of the local approach to fracture [10]. The method relies on finite element calculations of test pieces which are used to evaluate damage maps. These maps can then be used to predict crack initiation as well as crack direction of propagation (crack path).

Finite element calculations were carried out using axisymmetric or 3D elements with quadratic interpolation and reduced integration. Finite strain formalism is used. In regions where damage develops, a fixed element size (200 μm) was used.

6.1. Plastic behavior of the materials

The elasto-plastic behavior of the ferritic material can directly be obtained from the tensile tests. In order to obtain

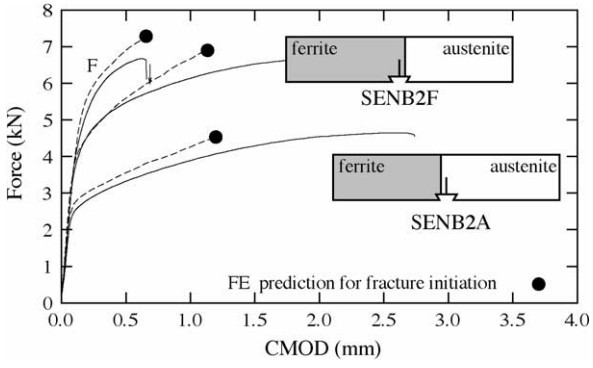

Fig. 12. SENB tests : force–CMOD curves for different samples. Dashed lines correspond to the FE simulation. Black dots indicate the predicted fracture initiation.

reliable data after the onset of necking, the Bridgman analysis [18] was used. Photographs were taken to directly measure the minimum cross section as well as the radius of curvature of the neck.

The plastic behavior of the austenite was determined using an inverse identification procedure. It was adjusted in order to match the mechanical response of sub–size homogeneous NT_{10} and heterogeneous NT_{χ} and NT_{V} samples. This identification strategy for the behavior of different materials is particularly interesting in the case of welds where it is difficult to obtain bulk material representative of the heat affected zone for instance. A similar procedure using notched samples was proposed in [17]. The identified hardening behavior is given by the following equation for the ferritic material (MPa):

$$\sigma_y(p) = 543 + 243(1 - \exp(-49.76p)) + 337(1 - \exp(-2.12p)), \quad (1)$$

and for the austenitic material by (MPa):

$$\sigma_y(p) = 259 + 1047(1 - \exp(-1.80p)) + 114(1 - \exp(-5.03p)), \quad (2)$$

where p is the equivalent von Mises plastic strain. All materials were assumed to be isotropic.

6.2. Evaluation of damage on notched bars (NT_{χ})

The damage of both materials is evaluated with a post-processor using the Rice and Tracey model for ductile void growth [19,10]. The original model is, however, only valid for high stress triaxiality [20]. The accuracy of the model was improved by Huang [21] in particular to better represent void dilatation rate at low stress triaxiality. In that case the void growth rate is given by

$$\frac{\dot{R}}{R} = \begin{cases} \alpha \exp(\beta\tau)\dot{p}, & \text{if } \tau > 1 \\ \alpha\tau^{1/4} \exp(\beta\tau)\dot{p}, & \text{if } \tau \leq 1 \end{cases} \quad \text{with} \quad \tau = \frac{\sigma_m}{\sigma_{eq}}, \quad (3)$$

where R is the void radius, σ_m the mean stress and σ_{eq} the equivalent von Mises stress. α and β are two constants equal to 0.427 and 1.5, respectively. Failure of a volume element is assumed to occur when void growth reaches a critical value $(R/R_0)_c$ (where R_0 is the initial void radius) which is assumed to be a material constant. A damage indicator (R/R_0) is obtained by integrating Eq. (3). The Rice and Tracey damage indicator was evaluated using averaged values of the plastic strain and the stress triaxiality ratio in each element. Numerical crack initiation is defined as the instant where the Rice and Tracey criterion is met for the first time in the structure. The crack extension at initiation corresponds to one element as averaged values are used.

The value of $(R/R_0)_c$ for the ferrite was adjusted to represent failure initiation on homogeneous smooth and notched tensile bars (TB, NT_{10}, NT_4, NT_2). Comparison of predicted failure with the experimental data is presented in Fig. 8(a) for $(R/R_0)_c$ equal to 2.14.

In the case of austenite, the following experiments were used: NT_{10}^{mini}, $NT_{10}I$ and $NT_{V}1A$. (Figs. 8(b) and 9(a)). The optimized critical void growth ratio is equal to 3.4. The Rice and Tracey criterion may be interpreted as a condition for void coalescence by internal necking [22]. As the austenite has the higher hardening rate, coalescence should occur for higher deformation levels than for the ferrite. This is consistent with its higher value for $(R/R_0)_c$. Fig. 9 shows damage maps at Gauss points for bimaterial notched bars. For the $NT_{10}I$ sample, the location of maximum damage is clearly situated below the interface and the simulation corresponds well to the examination of the fractured sample shown in Fig. 5(b). In the case of the NT_2I sample, high damage is located close to the interface which explains the interface debonding observed on this sample. In addition, faster growth of voids located at the interface, as shown in [23], may cause the debonding. This phenomenon is however not taken into account by the present model.

6.3. Finite element simulation of NT_{V} samples

Predicted failure initiation is shown in Fig. 9(b) for $NT_{2,3,4,6}F$ and NT_1A samples showing a good agreement. These tests were not used to adjust the critical void growth ratio and therefore validate the model. The damage map corresponding to sample NT_2F is also shown in the same figure showing that the crack initiates at the notch root and tends to deviate toward the interface. This corresponds to the observations reported in Fig. 5(c). The subsequent brittle fracture was not modeled in this study.

6.4. Finite element simulation of the Charpy and SENB specimens

Charpy and SENB tests were modeled using 3D calculations. It has been shown in the literature that the Charpy test cannot be modeled using plane strain or plane stress conditions [24,25] in the ductile regime. Contact between the sample, the support and the striker was also modeled assuming a friction coefficient equal to 0.1.

Results of the simulation are shown in Fig. 10 for cases where the V-notch lies in the ferrite and Fig. 11 for cases where the V-notch lies in the austenite. A good agreement is obtained comparing the force–displacement curves. Predicted failure initiation is also shown by the solid dots.

For the KCVF specimen, initiation occurs slightly before the maximum load. This corresponds to the fact that stable crack growth is observed. After the maximum load, the specimen fails by cleavage fracture. For KCV1F and KCV2F specimens, the maximum load level is reduced due to the deformation of the austenite. Initiation is delayed compared to homogeneous specimens.

For KCV#A specimens, initiation does not appear as being influenced by the presence of the hard ferritic material. This is partly due to the high hardening capacity of the austenite which prevents strain localization between the notch root and

the interface. Initiation occurs largely before the maximum load, as the 316L steel is extremely ductile and allows for very stable crack extension after initiation. Fig. 7(b) shows that crack extension remains limited at the maximum load.

Damage maps at initiation in the center of the specimen are also shown in Figs. 10 and 11. The crack path can be inferred from locations were damage is high. In the case of KCV1F and KCV2F specimens, damage tends to be higher toward the interface, which indicates crack deflection in this direction. The opposite effect is obtained for KCV1A and KCV2A specimens, which indicates that the crack propagates away from the interface. However, the effect is less marked than for KCV#F specimens. This corroborates well with the experimental results shown in Fig. 6.

Similar results are obtained from SENB specimens containing sharp fatigue cracks (Fig. 12) although the load tends to be overestimated. For homogeneous ferrite, ductile crack initiation is immediately followed by cleavage fracture; the predicted CMOD at initiation corresponds to the experimental failure. Note that the fatigue crack on the SENB specimen represents a more severe defect than the Charpy V-notch. For both SENB2F and SENB2A initiation is followed by stable crack growth. Crack deflections are similar to those observed for Charpy specimens.

7. Conclusions

In this study, diffusion bonded bi-material joints, consisting of austenite and ferrite, were investigated to analyze the effect of strength mismatch on damage growth, crack initiation and crack path close to the bi-material interface. Experiments were conducted on smooth and notched tensile bars, Charpy specimens and precracked SENB specimens on both homogeneous and heterogeneous structures with the geometrical defect being located in the austenite or the ferrite at different distances to the interface.

Tests on the different kinds of specimen consistently show that when the defect (crack or notch) is located in the ferrite, the overall ductility increases as the distance from the interface decreases whereas the load carrying capacity decreases. In addition, cracks tend to deflect toward the interface due to extensive plastic zone development in the austenite part. This mechanism could be of particular interest to stop propagating cracks in ferrite provided that the interface between both materials is strong enough. Opposite effects are observed when the defect is in the austenite, although crack deflection is less pronounced.

The observed variations of the ductility can be explained by the alterations of the stress state in the vicinity of the defect due to the strength mis-match. Compared to the homogeneous structure, the stress triaxiality ratio close to the defect is smaller (resp. larger) when the defect lies in the harder (resp. softer) material (see e.g. [5]). The variations of the limit load are structural effects which can be accounted for using finite element simulations (see e.g. [26]). Based on these observations, the different experiments can be simulated using models for ductile fracture coupled with structural computations. In this work, the simple Rice and Tracey model is used as a post-processor of elastoplastic calculations. The model parameter $((R/R_0)_c)$ for both materials is fitted on notched bars and validated on Charpy and SENB samples. In particular, the model can be used to interpret crack deflection in bi-material joints. A more detailed simulation including crack propagation would require the use of more sophisticated models coupling plastic hardening and damage growth such as the Rousselier [27] or Gurson [28] models.

References

[1] J. Rice, J. Appl. Mech. 35 (1968) 379.
[2] N. O'Dowd, C. Shih, J. Mech. Phys. Solids 39 (1991) 989–1015.
[3] N. O'Dowd, C. Shih, J. Mech. Phys. Solids 40 (1992) 939–963.
[4] A. Kim, S. Suresh, C. Shih, Int. J. Solids Struct. 34 (1997) 3415–3432.
[5] A. Kim, J. Besson, A. Pineau, Int. J. Solids Struct. 36 (1999) 1845–1864.
[6] Z. Zhang, C. Thawlow, M. Hauge, Eng. Fract. Mech. 57 (1997) 653–664.
[7] F. Beremin, Met. Trans. 12A (1981) 723–731.
[8] F.M. Beremin, Met. Trans. 14A (1983) 2277–2287.
[9] T. Moltubakk, C. Thaulow, Z. Zhang, Eng. Fract. Mech. 62 (1999) 445–462.
[10] A. Pineau, in: A. Argon (Ed.), Topics in Fracture and Fatigue, Springer Verlag Inc., NY, 1992, pp. 197–234.
[11] P. Joly, A. Pineau, in: Defect Assessment in Components—Fundamentals and Applications, Mechanical Engineering Publications, London, 1991, pp. 381–414.
[12] M. Isacsson, T. Narstrom, Mater. Sci. Eng. A 241 (1998) 169–178.
[13] T. Narstrom, M. Isacsson, Mater. Sci. Eng. A 271 (1999) 224–231.
[14] AFNOR, Essai de flexion par choc sur éprouvette Charpy. Partie 1: méthode d'essai, Association française de normalisation, La Défense, France, 1990.
[15] J. Besson, Mécanique et Ingénierie des Matériaux—Essais mécaniques—Éprouvettes axisymétriques entaillées, Hermes, 2001 pp. 319–351.
[16] K. Decamp, L. Bauvineau, J. Besson, A. Pineau, Int. J. Fract. 88 (1997) 1–18.
[17] Z. Zhang, M. Hauge, C. Thaulow, J. Ødegård, Eng. Fract. Mech. (2002) 353–366.
[18] P.W. Bridgman, Studies in large plastic flow and fracture, McGraw-Hill, 1952.
[19] J. Rice, D. Tracey, J. Mech. Phys. Solids 17 (1969) 201–217.
[20] M. Yatomi, A. Bettinson, N. O'Dowd, N. K.M., Fatigue Fract. Eng. Mater. Struct. 27 (2004) 283–295.
[21] Y. Huang, J. Appl. Mech. 58 (1991) 1084–1086.
[22] P.F. Thomason, J. Ins. Metals 96 (1968) 360.
[23] Z. Li, W. Guo, Int. J. Plast. 18 (2002) 249–279.
[24] K. Mathur, A. Needleman, V. Tvergaard, Modelling Simul. Mater. Sci. Eng. 1 (1993) 467–484.
[25] B. Tanguy, J. Besson, R. Piques, A. Pineau, Eng. Fract. Mech. 72 (2005) 413–434.
[26] Y. Kim, K. Schwalbe, Eng. Fract. Mech. 68 (2001) 1137–1151.
[27] G. Rousselier, Nucl. Eng. Des. 105 (1987) 97–111.
[28] V. Tvergaard, Adv. Appl. Mech. 27 (1990) 83–151.